AGU PUBLICATIONS

Geophysical Research Letters

RESEARCH LETTER
10.1002/2016GL069368

Key Points:
- Permanently shadowed regions (PSRs) identified in the north polar region of Ceres
- Northern PSR area is about 1800 km^2 based on topography-derived illumination model
- According to exosphere model calculations, fresh ice deposits are expected in the cold traps

Correspondence to:
N. Schorghofer,
norbert@hawaii.edu

Citation:
Schorghofer, N., E. Mazarico, T. Platz, F. Preusker, S. E. Schröder, C. A. Raymond, and C. T. Russell (2016), The permanently shadowed regions of dwarf planet Ceres, *Geophys. Res. Lett.*, *43*, 6783–6789, doi:10.1002/2016GL069368.

Received 27 APR 2016
Accepted 5 JUN 2016
Published online 6 JUL 2016

The permanently shadowed regions of dwarf planet Ceres

Norbert Schorghofer[1], Erwan Mazarico[2], Thomas Platz[3], Frank Preusker[4], Stefan E. Schröder[4], Carol A. Raymond[5], and Christopher T. Russell[6]

[1]Institute for Astronomy, University of Hawai'i at Mānoa, Honolulu, Hawaii, USA, [2]NASA Goddard Space Flight Center, Greenbelt, Maryland, USA, [3]Max Planck Institute for Solar System Research, Göttingen, Germany, [4]Deutsches Zentrum für Luft- und Raumfahrt (DLR), Berlin, Germany, [5]Jet Propulsion Laboratory, Pasadena, California, USA, [6]Department of Earth, Planetary, and Space Sciences, University of California, Los Angeles, California, USA

Abstract Ceres has only a small spin axis tilt (4°), and craters near its rotational poles can experience permanent shadow and trap volatiles, as is the case on Mercury and on Earth's Moon. Topography derived from stereo imaging by the Dawn spacecraft is used to calculate direct solar irradiance that defines the extent of the permanently shadowed regions (PSRs). In the northern polar region, PSRs cover ~1800 km^2 or 0.13% of the hemisphere, and most of the PSRs are cold enough to trap water ice over geological time periods. Based on modeling of the water exosphere, water molecules seasonally reside around the winter pole and ultimately an estimated 0.14% of molecules get trapped. Even for the lowest estimates of the amount of available water, this predicts accumulation rates in excess of loss rates, and hence, there should be fresh ice deposits in the cold traps.

1. Introduction

Ceres, Earth's Moon, and Mercury have a very small spin axis tilt, or obliquity, and low-lying topography (crater floors in particular) near the rotational poles can thus experience permanent shadow, where, due to low temperature, ices can accumulate [*Arnold*, 1979]. The Dawn spacecraft [*Russell and Raymond*, 2012] provides the first opportunity to explore permanently shadowed regions (PSRs) on Ceres. Here we use illumination calculations based on topographic data of the north polar region to determine the extent of the PSRs, and modeling is utilized to estimate how much ice may have accumulated in them.

Even permanent shadows receive indirect radiation, reflected sunlight at short wavelengths and reemitted thermal radiation at infrared wavelengths. The equilibrium temperature of a shadowed bowl-shaped crater can be calculated analytically using the formulas in *Buhl et al.* [1968] or *Ingersoll et al.* [1992] and happens to be uniform for this particular geometry. Given Ceres' low thermal inertia of ~15 J m^{-2} K^{-1} s$^{-1/2}$ [*Rivkin et al.*, 2011], the equilibrium temperature is a good approximation to the actual surface temperature. Figure 1 shows examples of the shadow temperature for two crater aspect ratios. The shallower the crater, the less reflected and reemitted radiance it receives, and the colder its shadow. Cold traps are conventionally defined as areas with peak surface temperature below 120 K. In the latitude range 70–90° (Sun elevations up to 24°), all PSRs in spherical craters of diameter to depth ratios of 5 or higher are cold traps for H_2O, unlike on the Moon and Mercury where only PSRs at the highest latitudes are sufficiently cold. Very near the poles of Ceres, other, non-H_2O ices can be trapped as well [*Hayne and Aharonson*, 2015].

2. Mapping of PSRs in the Northern Polar Region

Although the Dawn spacecraft observed Ceres' north pole near northern solstice, the temporal and spatial coverage obtained by the Framing Camera (FC) is naturally limited by orbit ground track and phasing, camera field of view, and data volume. Also the case for the Lunar Reconnaissance Orbiter [*Speyerer and Robinson*, 2013], this is especially true at Ceres given its relatively fast rotation rate (9.07417 h sidereal period). Computational modeling enables the mapping of solar illumination over the whole surface in any geometry, and thus the mapping of PSRs. Numerous such studies were conducted at the Moon and Mercury, with various kinds of topographic data sets and methods [e.g., *Bussey et al.*, 2010; *Mazarico et al.*, 2011].

Previous work at the Moon [*Mazarico et al.*, 2011] and Mercury [*Neumann et al.*, 2013] used a horizon method geared to low-obliquity bodies. *Stubbs and Wang* [2012] used a similar approach adapted to Vesta. Here we

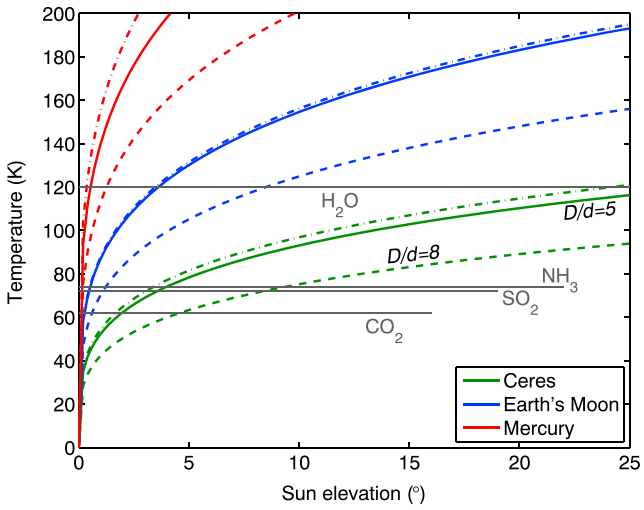

Figure 1. Theoretical equilibrium surface temperature of shadowed regions inside a bowl-shaped (spherical) crater. Solid lines are for a diameter-to-depth ratio $D/d=5$, the dash lines for $D/d=8$, and dash-dotted lines for $D/d=5$ and minimum Sun distance instead of the semimajor axis of the orbit around the Sun. The horizontal lines indicate cold trapping temperature limits for several volatiles as defined by a sublimation rate of 1 m/Ga [*Zhang and Paige*, 2009]. Respective Bond albedos of 0.034, 0.11, and 0.068 are used for Ceres, Earth's Moon, and Mercury.

chose an alternate method, direct ray tracing, used by *McGovern et al.* [2013] among others. The shape of Ceres is represented as a triangular mesh. For computational reasons, the size of the triangular elements increases with distance from the area of interest. The Sun is modeled as an extended two-dimensional disc, discretized in small elements with specific fluxes that account for limb darkening. Planetary positions and orientations are obtained through the SPICE toolkit [*Acton*, 1996], using kernels developed by the Dawn team. Both illumination (percentage of flux-weighted solar disc visible) and incident flux (accounting for incidence angle) are computed at each evaluation over all time steps. Following *Stubbs and Wang* [2012], we model the illumination conditions at 360 orbital positions of Ceres ($\Delta t \sim 4.7$ days), accounting for spin with 72 inner time steps ($\delta t \sim 7.5$ min). This reduces the number of illumination simulations to 25,920 compared to >320,000 to model a full Ceres orbit with a uniform time step δt.

We used the Ceres shape model obtained from High Altitude Mapping Orbit FC images [*Raymond et al.*, 2011] by Deutschen Zentrum für Luft- und Raumfahrt through stereo-photogrammetry (SPG) [*Preusker et al.*, 2016], and associated orientation parameters (spin period and pole position). The simulations were carried out at 500 m/pixel resolution. Figure 2 shows a validation of the illumination model.

Figure 3 shows the results of the illumination simulation with the preferred SPG model, showing the maximum incident flux on the surface over a Cerean year. PSRs, in red, are located mostly on pole-facing crater walls or parts of crater floors. No significant (at the 2 σ level) asymmetry exists in longitude. Unlike the Moon where the proportion of the surface in permanent shadow above a given latitude increases toward the pole, the fractional area in permanent shadow is maximum on Ceres over the 80°–90°N cap. The Moon also has more and particularly deep impact craters in the 80°S–90°S region.

Given the distortion of the polar stereographic projection, the area of a pixel is

$$\Delta A = \frac{4R^2}{4k_0^2R^2 + x^2 + y^2} \tag{1}$$

where x, y are the pixel coordinates measured from the north pole, R the projection radius (km), and k_0 the scale at the pole (pixel/km).

The cumulative area of the PSRs in our study area is ~1800 km^2. This corresponds to 0.129% of the hemisphere for a rotational ellipsoid 482 × 446 km [*Preusker et al.*, 2016]. The largest single cold trap resides within a ~16 km diameter crater centered at 82°N, 77°E.

For Mercury, the PSR area poleward of 69°N is 0.124% [*Neumann et al.*, 2013]. For the Moon [*Mazarico et al.*, 2011], the PSR area is 0.157% for the southern hemisphere and 0.144% for the northern hemisphere (65–90°). The relative proportion of PSRs on Ceres is comparable to Mercury but lower than on the Moon, at least based on northern hemisphere results. Before Dawn's arrival at Ceres, *Hayne and Aharonson* [2015] predicted that 0.4% of Ceres' surface are cold traps located above 60° latitude, at finer spatial resolution. Due to seasonal illumination conditions during the Dawn primary mission at Ceres, PSRs in the southern hemisphere are not well constrained by Dawn observations.

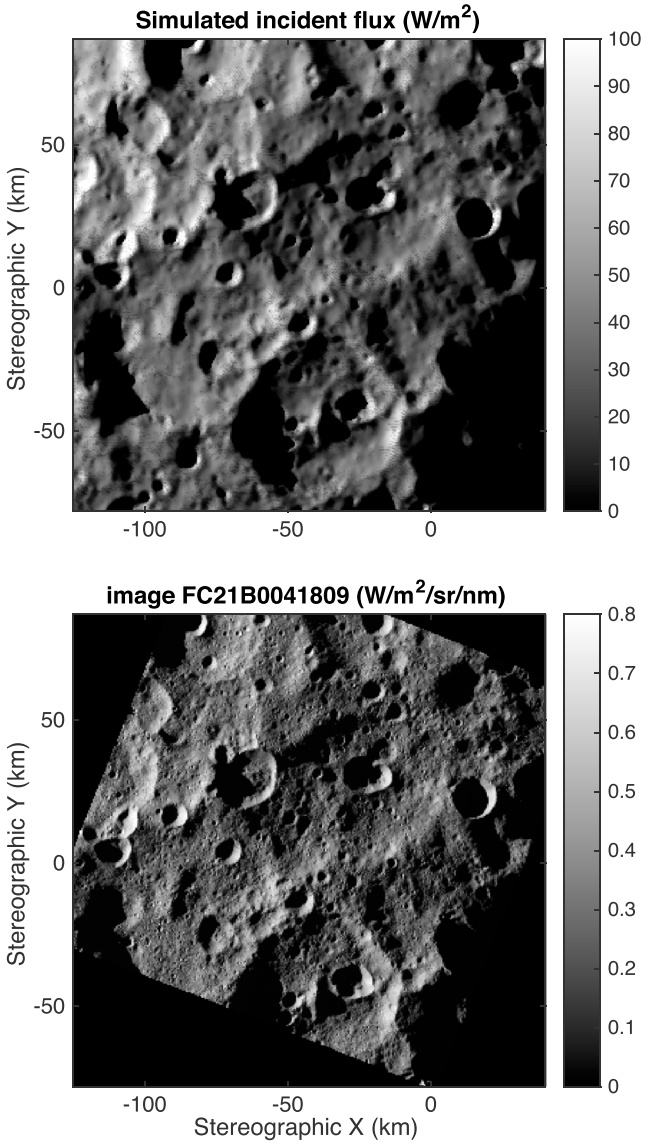

Figure 2. Instantaneous illumination calculated from the SPG shape model of Ceres compared with the shadows in an FC image. Axes are in kilometers, using a north polar stereographic projection with a radius of 470 km.

3. Model of Water Exosphere and Ice Accumulation

Ceres' gravity is strong enough to maintain a surface-bounded exosphere with molecules that travel on ballistic trajectories. In this way, H_2O molecules can migrate from any part of the surface to the cold traps [*Tu et al.*, 2014].

To determine the fraction of molecules trapped instead of lost, a Monte Carlo model of ballistic hops is used. Hop distance and time of flight are calculated for nonuniform gravity and a rotating sphere. Analytical equations for time of flight and launch and landing coordinates are used. The Coriolis effect is incorporated by adding tangential velocities but subtracting the distance the surface has traveled during time of flight. Molecules leave the surface at thermal speed and with a Gaussian velocity distribution. Surface temperature is obtained from a dynamic thermal model, a global grid of one-dimensional heat equations at each longitude-latitude point. Molecular residence times on the surface are estimated based on sublimation rates and become large compared to the length of the solar day at temperatures below about 130 K. The photodestruction rate for normal Sun activity at 1 AU [*Crovisier*, 1989] is divided by the square of the semimajor axis, $1.6\times10^{-6}\,s^{-1}$. Model code and detailed equations can be found in *Schorghofer* [2016a].

The thermal speed of water molecules is comparable to Ceres' escape speed (0.52 km/s), and hop lengths are comparable to the size of Ceres. A large fraction of molecules escape the gravity field, a small fraction is destroyed by photodissociation, and an even smaller fraction lands in a PSR and is cold trapped. Even the small axis tilt (approximately 4° [*Preusker et al.*, 2016; *Ermakov et al.*, 2016]) causes a seasonal effect, where water molecules seasonally reside near the winter pole, although this frost is not thick enough to lead to an observable change in surface albedo. This necessitates that model calculations of the exospheric transport have to be run for not only a few solar days but over at least one whole orbit to determine the average cold trapping fraction.

Over 6600 solar days (roughly 1.5 orbits) are modeled, and results from the last Cerean year are used to calculate the average trapping and loss rates. The water source is assumed to be the equatorial region, between −40° and +40° latitude, where most of the ice retreat occurs, but because the hop lengths are so large the location of the source plays only a minor role. The water supply is assumed to be steady in time. Likewise, the exact locations of the cold traps play only a minor role and the cold trapping area is lumped together into a circular disc around each pole. Calculations with a ring-shaped cold trap with the same area centered at a latitude of 80° yielded the same results. Nearly 4×10^6 computational particles were tracked, although no more than 20,000 at any time.

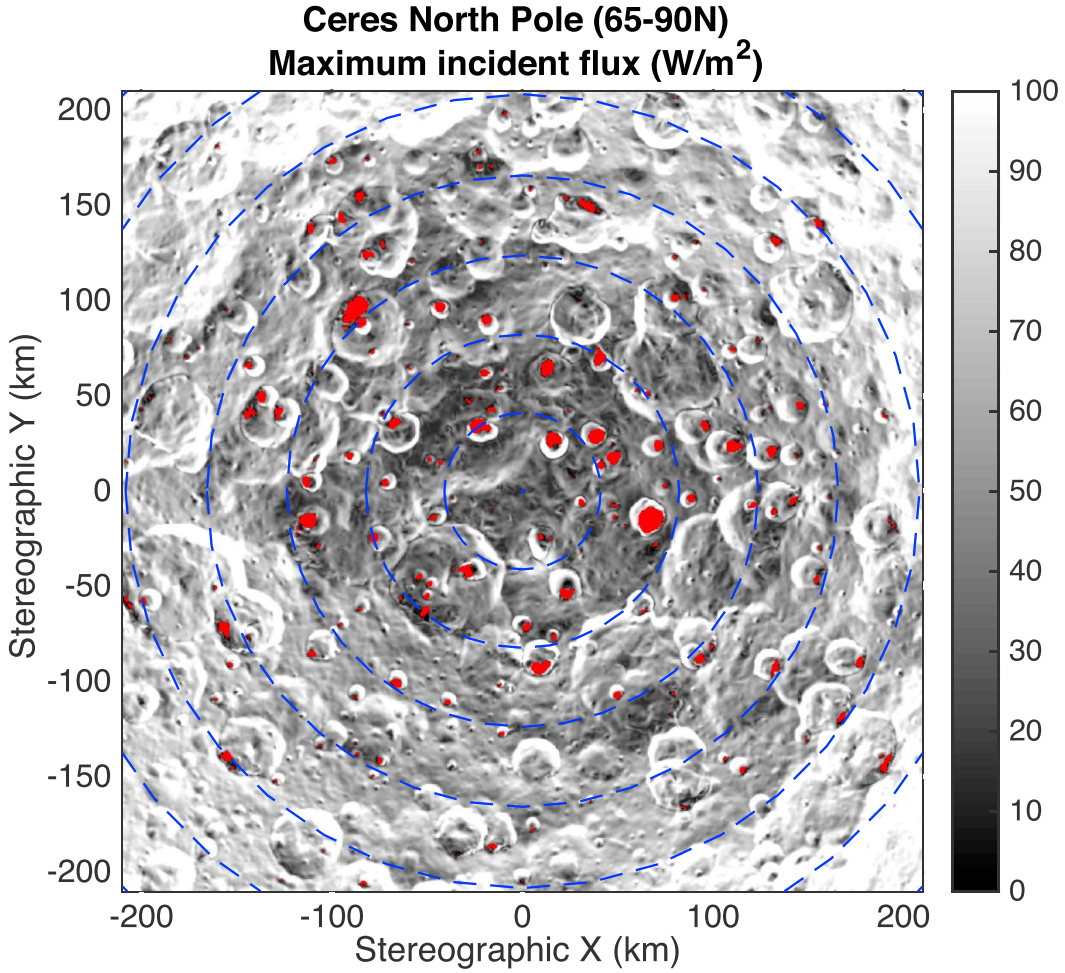

Figure 3. Maximum direct illumination in the north polar region of Ceres. Latitudes 65–90°N are shown in this polar stereographic projection, and the lowest latitude in the corners of the square region is ~55°N. Dashed circles are spaced in intervals of 5° latitude. The irradiance is determined from ray tracing calculations based on the SPG shape model.

For the estimated cold trapping area of 0.13%, mirrored on the south pole, 0.14% of the water molecules that are generated on the surface end up in the cold traps over a Cerean year. About 91% of molecules are lost due to gravitational escape, and nearly 9% to photodestruction. The median number of hops before a molecule is either lost or cold trapped is three. The median flight duration, for molecules that land again, is 81 min.

Figure 4 shows the results of exosphere model calculations for Ceres, the Moon, and Mercury. The fraction of molecules trapped is almost as high as on Mercury, but much lower than on the lunar surface [*Schorghofer*, 2014; *Moores*, 2016]. To determine the influx of water molecules to the cold traps (and thus the thickness of the deposits), only the ratio of the fraction trapped to the fraction of cold trap area matters. For Ceres, this ratio is nearly independent of the total cold trapping area. This "cold trapping efficiency" is 1.1. The thickness of ice deposits for a given amount of available water is hence nearly independent of the cold trapping area.

Ceres has an ice-rich crust [*Prettyman et al.*, 2016] that gradually retreats and feeds an exosphere. Based on model calculations of retreating ice, *Fanale and Salvail* [1989] estimated that the current global water supply rate is 0.03–0.30 kg/s, and *Schorghofer* [2016b] estimated that 0.2 kg/s of H_2O is currently output as a direct result of the globally retreating ice; these estimates depend on assumptions about the physical properties of the top tens of meters. *Rousselot et al.* [2011] placed an upper bound of $\sim 7 \times 10^{25}$ molecules/s (0.3 kg/s), based on the lack of observed OH, the dissociation product of H_2O. Observations by the Herschel telescope suggest an output of 6 kg/s [*Küppers et al.*, 2014], but such a high rate is unlikely to be maintained in the long term, because of the large volume of ice it would consume.

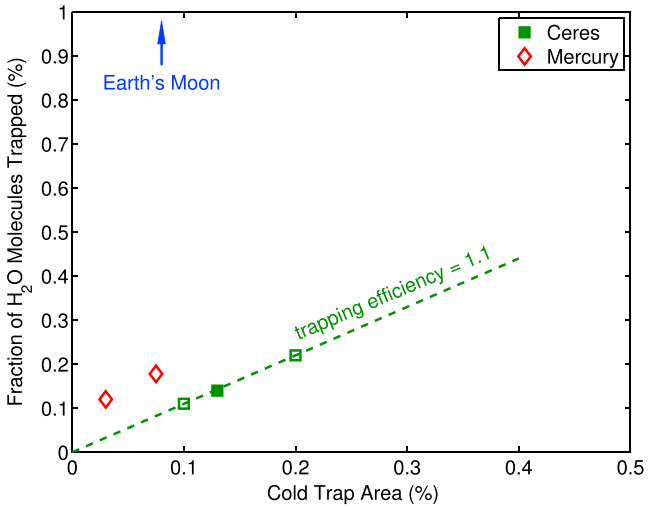

Figure 4. Fraction of water molecules trapped versus cold trapping area based on model calculations of the water exosphere. The proportionality constant is the "trapping efficiency." The trapping fraction for the Moon is off scale (about 11%).

The influx of water molecules into the cold traps is the source flux (per global surface area) multiplied by the unitless trapping efficiency. With a trapping efficiency of 1.1 and for the lowest of the supply estimates of 0.03 kg/s, 0.4 m of ice should have accumulated over the last Gyr alone. This rate is higher than the estimated Lyman α space weathering erosion rate of ~0.1 m/Gyr [*Morgan and Shemansky*, 1991]. The impact gardening rate on Ceres is not known. The lunar gardening rate is 0.1 m/Gyr [*Gault et al.*, 1974]; impacts on Ceres are expected to be more frequent but slower, so that the gardening depth may be similar. Hence, fresh (and thus potentially optically bright) ice deposits can be expected in the cold traps, even without any additional water delivery from infall or other sources. That said, the gardening rate, the space weathering erosion rate, and the minimum supply rate are only estimates.

4. Discussion

The axis tilt (obliquity) of Ceres may vary over time, which can lead to loss of ice from areas that are currently PSRs. Assuming a fully damped spin state and the shape parameters available at the time, *Bills and Nimmo* [2011] estimated that the obliquity would vary between about 10° and 12° with a period on the order of 100 kyr. *Rambaux et al.* [2011] estimated the timescale for the spin axis orientation to relax to a generalized Cassini state and found that internal tidal dissipation has probably been too small to drive any significant damping of its obliquity since formation. Little definite can be said so far about excursions beyond the current 4° value. The systematic change of the power spectrum of the topography with latitude suggests that at least no true polar wander took place [*Ermakov et al.*, 2016].

Shadowed regions in shallow craters are colder than shadowed regions in craters with smaller aspect ratios, but on Ceres even diameter-to-depth ratios of 5 can be expected to be cold traps (Figure 1). Craters on Ceres often have higher diameter-to-depth ratios than the canonical ratio of 5 [*Schenk et al.*, 2016]. These crater geometries are relatively robust to spin axis variations. Moreover, even if cold traps were destroyed during a recent obliquity excursion, over a period of a mere 100 kyr, many microns of water should have newly accumulated, possibly forming an optically thick layer.

On Mercury, the cold traps are filled with water ice [*Slade et al.*, 1992; *Lawrence et al.*, 2013; *Neumann et al.*, 2013; *Paige et al.*, 2013; *Chabot et al.*, 2014]. On the Moon, the circumstances are more complex [e.g., *Feldman et al.*, 1998; *Zuber et al.*, 2012; *Hayne et al.*, 2015]. The origin of the ice in the cold traps of Mercury and the Moon is not known and could be exogenic (infall from comets, meteorites, or interplanetary dust particles) or endogenic (solar wind generated or outgassing). For Ceres, the retreating subsurface ice layer is another source for cold trapped water.

Infall of H_2O-bearing material can be expected to be higher on Ceres than on Mercury and the Moon, due to its location in the asteroid belt. Solar wind-generated H_2O, on the other hand, would rapidly decrease with distance from the Sun. The chemical mechanisms that may lead to the formation of H_2O from the interaction of solar wind protons with the surface are not fully understood and may even involve a temperature threshold that Ceres does not exceed [*Poston et al.*, 2013].

Incidentally, the trapping efficiency on Mercury and Ceres are similar; that is, for the same number of generated water molecules per surface area, the thickness of the ice accumulating in the cold traps should be almost as high on Ceres than on Mercury. Hence, significant differences in the thickness of young ice deposits

may reveal the main source of water. A lack of ice deposits in Cerean cold traps would suggest that infall is not a major source of this ice, consistent with a solar wind generation mechanism on Mercury.

5. Conclusions

Based on illumination calculations derived from topography, the permanently shadowed regions in the northern hemisphere of Ceres cover 1800 km^2 or 0.13% of the hemisphere. The relative PSR area is similar to Mercury, but unlike Mercury most of these areas are cold enough to serve as efficient cold traps for water ice.

Based on modeling of the water exosphere, averaged long enough to take into account seasonal condensation around the winter pole, the trapping efficiency of H_2O (ratio of the fraction of molecules trapped to the fractional cold trap area) is 1.1. With an estimated global cold trap area of 0.13%, 0.14% of water should get trapped. Incidentally, this is roughly comparable to the fraction trapped on Mercury. Combined with the lowest estimated supply rates, from retreating ice without exogenic sources, this yields accumulation rates in excess of estimated space weathering rates and in excess of typical (lunar) gardening depths. Hence, fresh, and thus potentially optically bright, ice deposits can be expected in the cold traps, even without any additional water delivery.

Direct measurements of the amount of ice in the cold traps of Ceres could provide constraints on the origin of ice in the cold traps of Mercury and the Moon, as well as for the spin axis history of Ceres.

Acknowledgments
We thank the Dawn team for the acquisition and processing of data used in this work. N.S. was supported by the National Aeronautics and Space Administration under grant NNX15AI38G issued through the Dawn at Ceres Guest Investigator Program (DACGIP). E.M. also acknowledges support from DACGIP.

References

Acton, C. H. (1996), Ancillary data services of NASA's navigation and ancillary information facility, *Planet. Space Sci.*, *44*(1), 65–70.
Arnold, J. R. (1979), Ice in the lunar polar regions, *J. Geophys. Res.*, *84*(B10), 5659–5668.
Bills, B. G., and F. Nimmo (2011), Forced obliquities and moments of inertia of Ceres and Vesta, *Icarus*, *213*(2), 496–509.
Buhl, D., W. J. Welch, and D. G. Rea (1968), Reradiation and thermal emission from illuminated craters on the lunar surface, *J. Geophys. Res.*, *73*, 5281–5295.
Bussey, D. B. J., et al. (2010), Illumination conditions of the south pole of the Moon derived using Kaguya topography, *Icarus*, *208*, 558–564.
Chabot, N. L., et al. (2014), Images of surface volatiles in Mercury's polar craters acquired by the MESSENGER spacecraft, *Geology*, *42*(12), 1051–1054.
Crovisier, J. (1989), The photodissociation of water in cometary atmospheres, *Astr. Astrophys.*, *213*, 459–464.
Ermakov, A., M. Zuber, D. Smith, R. Fu, C. Raymond, R. Park, and C. Russell (2016), Evaluation of Ceres' compensation state, in *Lunar and Planetary Science Conference*, vol. 47, LPI Contrib. No. 1903, Abstract 1708, Woodlands, Tex.
Fanale, F. P., and J. R. Salvail (1989), The water regime of asteroid (1) Ceres, *Icarus*, *82*, 97–110.
Feldman, W. C., S. Maurice, A. B. Binder, B. L. Barraclough, R. C. Elphic, and D. J. Lawrence (1998), Fluxes of fast and epithermal neutrons from Lunar Prospector: Evidence for water ice at the lunar poles, *Science*, *281*(5382), 1496–1500.
Gault, D. E., F. Hoerz, D. E. Brownlee, and J. B. Hartung (1974), Mixing of the lunar regolith, in *5th Lunar Science Conference*, pp. 2365–2386, Pergamon Press, Inc., New York.
Hayne, P. O., and O. Aharonson (2015), Thermal stability of ice on Ceres with rough topography, *J. Geophys. Res. Planets*, *120*, 1567–1584, doi:10.1002/2015JE004887.
Hayne, P. O., A. Hendrix, E. Sefton-Nash, M. A. Siegler, P. G. Lucey, K. D. Retherford, J.-P. Williams, B. T. Greenhagen, and D. A. Paige (2015), Evidence for exposed water ice in the Moon's south polar regions from Lunar Reconnaissance Orbiter ultraviolet albedo and temperature measurements, *Icarus*, *255*, 58–69.
Ingersoll, A. P., T. Svitek, and B. C. Murray (1992), Stability of polar frosts in spherical bowl-shaped craters on the Moon, Mercury, and Mars, *Icarus*, *100*(1), 40–47.
Küppers, M., et al. (2014), Localized sources of water vapour on the dwarf planet (1) Ceres, *Nature*, *505*(7484), 525–527.
Lawrence, D. J., et al. (2013), Evidence for water ice near Mercury's north pole from MESSENGER Neutron Spectrometer measurements, *Science*, *339*(6117), 292–296.
Mazarico, E., G. A. Neumann, D. E. Smith, M. T. Zuber, and M. H. Torrence (2011), Illumination conditions of the lunar polar regions using LOLA topography, *Icarus*, *211*, 1066–1081.
McGovern, J. A., D. B. Bussey, B. T. Greenhagen, D. A. Paige, J. T. S. Cahill, and P. D. Spudis (2013), Mapping and characterization of non-polar permanent shadows on the lunar surface, *Icarus*, *223*(1), 566–581.
Moores, J. E. (2016), Lunar water migration in the interval between large impacts: Heterogeneous delivery to permanently shadowed regions, fractionation, and diffusive barriers, *J. Geophys. Res. Planets*, *121*, 46–60, doi:10.1002/2015JE004929.
Morgan, T. H., and D. E. Shemansky (1991), Limits to the lunar atmosphere, *J. Geophys. Res.*, *96*(A2), 1351–1367.
Neumann, G. A., et al. (2013), Bright and dark polar deposits on Mercury: Evidence for surface volatiles, *Science*, *339*(6117), 296–300.
Paige, D. A., et al. (2013), Thermal stability of volatiles in the north polar region of Mercury, *Science*, *339*(6117), 300–303.
Poston, M. J., G. A. Grieves, A. B. Aleksandrov, C. A. Hibbitts, M. D. Dyar, and T. M. Orlando (2013), Water interactions with micronized lunar surrogates JSC-1A and albite under ultra-high vacuum with application to lunar observations, *J. Geophys. Res. Planets*, *118*(1), 105–115, doi:10.1002/jgre.20025.
Prettyman, T., et al. (2016), Elemental composition of Ceres by Dawn's Gamma Ray and Neutron Detector, in *Lunar and Planetary Science Conference*, vol. 47, LPI, Abstract 2228.
Preusker, F., F. Scholten, K.-D. Matz, S. Elgner, R. Jaumann, T. Roatsch, S. P. Joy, C. A. Polanskey, C. A. Raymond, and C. T. Russell (2016), Dawn at Ceres—Shape model and rotational state, in *Lunar and Planetary Science Conference*, vol. 47, LPI, Abstract 1954.
Rambaux, N., J. Castillo-Rogez, V. Dehant, and P. Kuchynka (2011), Constraining Ceres' interior from its rotational motion, *Astron. Astrophys.*, *535*, A43.
Raymond, C. A., et al. (2011), The Dawn topography investigation, *Space Sci. Rev.*, *163*(1), 487–510, doi:10.1007/s11214-011-9863-z.

Rivkin, A. S., J.-Y. Li, R. E. Milliken, L. F. Lim, A. J. Lovell, B. E. Schmidt, L. A. McFadden, and B. A. Cohen (2011), The surface composition of Ceres, *Space Sci. Rev.*, *163*, 95–116.
Rousselot, P., E. Jehin, J. Manfroid, O. Mousis, C. Dumas, B. Carry, U. Marboeuf, and J.-M. Zucconi (2011), A search for water vaporization on Ceres, *Astron. J.*, *142*(4), 125.
Russell, C. T., and C. A. Raymond (2012), *The Dawn Mission to Minor Planets 4 Vesta and 1 Ceres*, 574 pp., Springer, New York.
Schenk, P., et al. (2016), Impact cratering on the small planets Ceres and Vesta: SC transitions, central pits, and the origin of bright spots, in *47th Lunar and Planetary Science Conference*, vol. 47, LPI, Abstract 2697.
Schorghofer, N. (2014), Migration calculations for water in the exosphere of the Moon: Dusk-dawn asymmetry, heterogeneous trapping, and D/H fractionation, *Geophys. Res. Lett.*, *41*, 4888–4893, doi:10.1002/2014GL060820.
Schorghofer, N. (2016a), Planetary-Code-Collection: Thermal and ice evolution models for planetary surfaces v1.1.1, *GitHub*, doi:10.5281/zenodo.48851.
Schorghofer, N. (2016b), Predictions of depth-to-ice on asteroids based on an asynchronous model of temperature, impact stirring, and ice loss, *Icarus*, *276*, 88–95.
Slade, M. A., B. J. Butler, and D. O. Muhleman (1992), Mercury radar imaging—Evidence for polar ice, *Science*, *258*, 635–640.
Speyerer, E. J., and M. S. Robinson (2013), Persistently illuminated regions at the lunar poles: Ideal sites for future exploration, *Icarus*, *222*(1), 122–136.
Stubbs, T. J., and Y. Wang (2012), Illumination conditions at the Asteroid 4 Vesta: Implications for the presence of water ice, *Icarus*, *217*(1), 272–276.
Tu, L., W.-H. Ip, and Y.-C. Wang (2014), A sublimation driven exospheric model of Ceres, *Planet. Space Sci.*, *104*, 157–162.
Zhang, J. A., and D. A. Paige (2009), Cold-trapped organic compounds at the poles of the Moon and Mercury: Implications for origins, *Geophys. Res. Lett.*, *36*, L16203, doi:10.1029/2009GL038614.
Zuber, M. T., et al. (2012), Constraints on the volatile distribution within Shackleton crater at the lunar south pole, *Nature*, *486*, 378–381.